Review of Scientific Instruments

Nondestructive measurements of depth distribution of carrier lifetimes in 4H-SiC thick epitaxial layers using time-resolved free carrier absorption with intersectional lights

Takashi Hirayama[1], Keisuke Nagaya[1], Akira Miyasaka[2], Kazutoshi Kojima[3], Tomohisa Kato[3], Hajime Okumura[3], Masashi Kato[1,4*]

1. Department Electrical and Mechanical Engineering, Nagoya Institute of Technology, Nagoya 466-8555, Japan

2. SHOWA DENKO K.K., 1-13-9, Shibadaimon, minato, Tokyo 105-0012, Japan

3. National Institute of Advanced Industrial Science and Technology (AIST), 1-1-1 Umezono, Tsukuba, Ibaraki 305-8568, Japan

4. Frontier Research institute for Materials Science, Nagoya Institute of Technology, Nagoya 466-8555, Japan

* kato.masashi@nitech.ac.jp

To achieve low on-state and switching losses simultaneously in SiC bipolar devices, the depth distribution of the carrier lifetime within the voltage blocking layer and the techniques used for observing the carrier lifetime distribution are important considerations. We developed a measurement system of the time-resolved free carrier absorption with intersectional lights (IL-TRFCA) for the nondestructive measurements of the depth distribution of the carrier lifetime in 4H-SiC thick epilayers. To confirm reliability of the measurement results, we also performed TRFCA measurements to cross-section of the samples. As a result, although the lifetimes are underestimated owing to an inevitable diffusion of the carriers from the measurement region, the system was able to observe a carrier lifetime distribution up to a depth of 250 μm. Our IL-TRFCA system demonstrated a depth resolution of ~10 μm, which is the best resolution among previously reported nondestructive measurement techniques. We consider the proposed system to be useful for the development of SiC bipolar devices.

Introduction

Owing to its high breakdown electric field and moderate electron mobility, 4H-SiC is a promising material for low-loss and high-voltage power devices.[1,2] Schottky barrier diodes (SBDs) and metal oxide semiconductor field effect transistors (MOSFETs) using 4H-SiC within a voltage range of 0.6–3.3 kV have become commercially available. This voltage range is suitable for vehicles, trains, and home electronics. By contrast, devices used in power systems usually operate within a higher voltage range, and

in some cases, the required voltage will be higher than 10 kV. Under a high voltage range, SBDs and MOSFETs, which are unipolar devices, show significant on-state power losses from their relatively high on-resistances owing to the requirement of a thick voltage blocking layer. To reduce the on-state power losses, the adoption of bipolar device structures is effective because such structures have a relatively low on-resistance from the conductivity modulation.[4–7] The effects of the conductivity modulation depend on the carrier lifetime, and a long carrier lifetime in the voltage blocking layer enhances the effects of the conductivity modulation. By contrast, the longer carrier lifetime induces a higher switching loss owing to the minority carrier accumulation effect. To achieve a low on-state and switching losses simultaneously, control of the distribution of the carrier lifetime in the voltage blocking layer has been frequently employed.[8,9] Therefore, the depth distribution of the carrier lifetime in an epitaxially grown voltage blocking layer is important for SiC bipolar devices. In addition, the depth distribution of the carrier lifetime is important even for MOSFETs when power electronic circuits employ body pn diodes. Minority carriers are injected from the anodes of the body diodes during a diode operation. If the injected minority carriers recombine with electrons at the basal plane dislocations (BPDs), partial dislocations of the BPDs will become mobile, resulting in an expansion of single Shockley stacking faults (1SSFs). For suppression of the 1SSF expansion, the insertion of a short carrier lifetime layer, called a recombination enhancing layer (REL), between the voltage blocking layer and the substrate has been suggested.[10] Therefore, information of the carrier lifetime distribution in the epitaxial layers for a MOSFET is also important.

The depth distributions of the carrier lifetime have usually been observed by cross-sectional surfaces of the samples or repeated carrier lifetime measurements and a thinning of the samples.[11–14] In such cases, the sample was destroyed from the original wafers, and after the observation, the samples were therefore unable to be used for a device fabrication. Thus, demand exists for the development of nondestructive techniques to observe the depth distribution of the carrier lifetime, although thus far only two nondestructive techniques have been reported. One is based on time-resolved photoluminescence with

two-photon absorption (TPA-TRPL),[15] and the other is based on time-resolved free carrier absorption (TRFCA) with intersectional arrangement of the excitation and probe lights (IL-TRFCA).[16] Although its spatial resolution is not as high owing to a carrier diffusion that occurs during the measurements, the TPA-TRPL technique has an advantage owing to an accurate estimation of the carrier lifetimes through a fitting with a model of the carrier diffusion. By contrast, IL-TRFCA has an advantage of a spatial resolution owing to an independent observation region of the carrier diffusion but has difficulty in accurately estimating the carrier lifetime owing to a diffusion of the carriers from the observation region. Therefore, these can be considered complemental techniques. However, our previous report on IL-TRFCA showed only the results of epilayers of thinner than 100 μm, which corresponds to voltage blocking layers for devices of less than 10 kV. Therefore, to assist in the development of bipolar SiC devices, we need to improve the IL-TRFCA for observations of thicker epilayers. In this study, we report an improved IL-TRFCA system for achieving a higher signal-to-noise ratio in measurements of deep regions within thick epilayers.

Experiments

For the TRFCA measurements, we employed a 355-nm pulsed yttrium aluminum garnet (YAG) laser (pulse width of 1 ns) as an excitation light, and 405- and 637-nm continuous wave (CW) lasers as probe lights. Both laser lights were focused on the sample using an objective lens with a numerical aperture (NA) of 0.65, which is larger than that of the lens employed in a previous study.[16] We used two different optical path configurations: intersection (IL-TRFCA) and cross-section (normal TRFCA) configurations. In both measurements, temporal resolution is ~2 ns due to pulse width of the laser and 1 GHz bandwidth of the oscilloscope. We normalized the peak of the FCA signal to 1, and we defined the 1/e lifetime as a signal decay time from a peak to 1/e.

In intersection measurements, the diameters of both lasers at the focal points were ~3 μm. The optical paths of both lasers on the sample were designed with incident angles of 34° and −34° by inducing the laser lights at edges of the objective lens pupil, as shown in Fig. 1(a), which are larger angles compared with the previous system for increasing the spatial resolution in the depth direction. We employed a 405-nm probe light to suppress the difference in the refractive indices from the excitation light (refractive indices of 4H-SiC at 355 and 405 nm are 2.83 and 2.75, respectively[17]). During the measurements, the sample was moved toward the objective lens at intervals of 0.5 or 1 μm. Owing to the difference in the refractive indexes between air and the sample, the measurement positions were nearly 3.3-times deeper than the movement of the sample, as shown Fig. 1(b). The intensity of the excitation light decreased in the sample owing to the absorption. The intensity is given by the following:

$$\boldsymbol{P = P_0 \exp(-\alpha X)}, \tag{1}$$

where P is the intensity at the measurement position; P_0 is the intensity at the sample surface; α is the absorption coefficient of the sample, which is ~200 cm^{-1} for 4H-SiC at 355 nm;[18] and X is the optical distance from the surface to the measurement position as shown in Fig. 1(c), and can be expressed as follows:

$$\boldsymbol{X = \frac{z}{\sqrt{\frac{1}{n^2} - \left(\frac{\sin(\theta_{in})}{n}\right)^2}} = \frac{nz}{\cos(\theta_{in})}}. \tag{2}$$

Here z is the movement of the sample, n is the refractive index of the sample, and θ_{in} is the incident angle of the excitation light. To maintain a constant P, we increased the intensity of the excitation light (P_0) through an increase in the measurement depth by rotating a half-wavelength plate against a polarizing beam splitter on the optical pass. In this study, we arranged the number of injected photons 10^{16} cm^{-2} at the measurement positions. This injection excited ~10^{18} cm^{-3} of carriers around the measurement positions,

and, in this concentration, there will be almost negligible contribution of the Auger recombination in a decay of carriers.[19] By contrast, the probe light transmitted through the sample was detected using a silicon photodiode (Si PD) through a condenser lens (NA = 0.79), which was not employed in the previous study.[16] Even though we arranged the angle of the probe light as 34°, the angle of the transmitted light was not stable during the measurements due to imperfect flatness of the sample surfaces. By the utilization of this high NA lens, we were able to collect the probe light throughout the measurements. A long pass filter used to block the excitation light (355 nm LPF) and a band pass filter for 405-nm light (405-nm BPF) are placed in front of the Si PD. Even though diameters of the laser spots at the focal point were ~3 μm, the lateral spatial resolution of this measurement will be more than 10 μm considering the imperfect flatness of the sample surface and carrier diffusion.

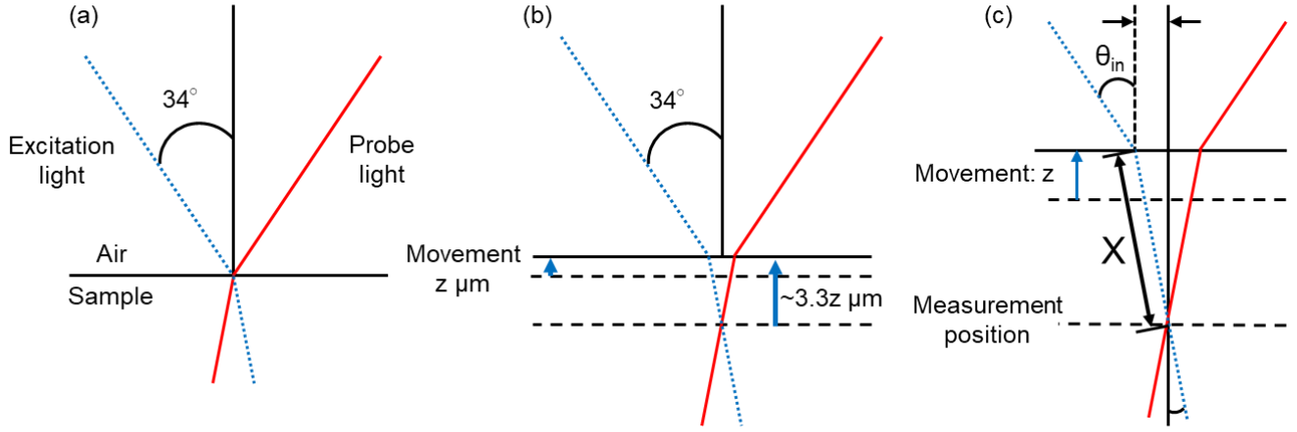

Fig. 1. Cross-section schematics of the intersection measurements: (a) both laser lights focused onto the surface of the sample with incident angles of 34° and –34° using an objective lens, (b) the sample moved 5-μm toward the objective lens, and (c) the vicinity of the measurement position.

For the cross-section measurements, the laser diameters of the excitation and probe lights are 56 and ~1 μm respectively. The laser lights were induced at the center of the objective lens pupil and paths of both lasers were normal to the cross-sectional surface of the sample. To enhance the signal-to-noise ratio,

the wavelength of the probe light was 637 nm, which is absorbed more by the free carriers than the 405-nm light.[20,21] The sample was moved in the depth direction during the measurements, and the number of injected photons for excitation was 10^{16} cm^{-2} as same as the intersection measurements. The probe light transmitted through the sample was detected using a Si PD through a plano-convex lens (NA = 0.13), a 355-nm LPF, and a 637-nm BPF. In this cross-section measurement, the angle of transmitted light was stably normal to the sample during the measurements and then we adopted the plano-convex lens with a longer working distance than the condenser lens in the intersection measurement. The optical path of the cross-section measurement was as schematically shown in Fig. 2. Considering this optical path and penetration depth of the excitation light (~42 μm), the spatial resolution of the cross-section measurement will be ~10 μm.[22] Figure 3 shows a photograph of our proposed TRFCA system, which was employed for both the intersection and cross-section measurements. We were able to select one of the CW lasers and to vary diameters and positions against the objective lens of the laser light by using apertures and mirrors.

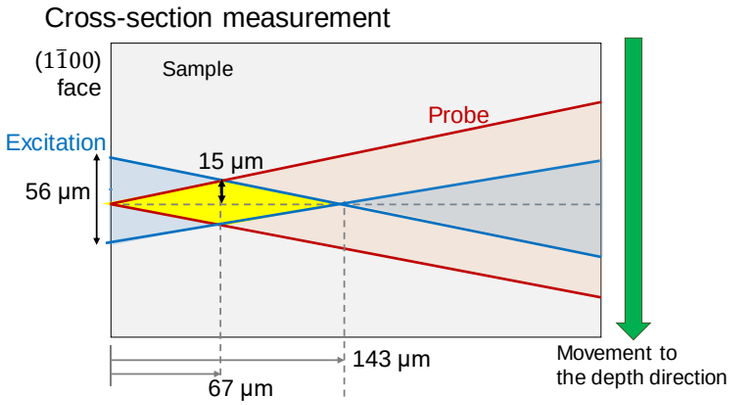

Fig. 2. Schematic of the optical path for the cross-section measurements. We employed 2.63 as the refractive index of 4H-SiC for 637 nm.

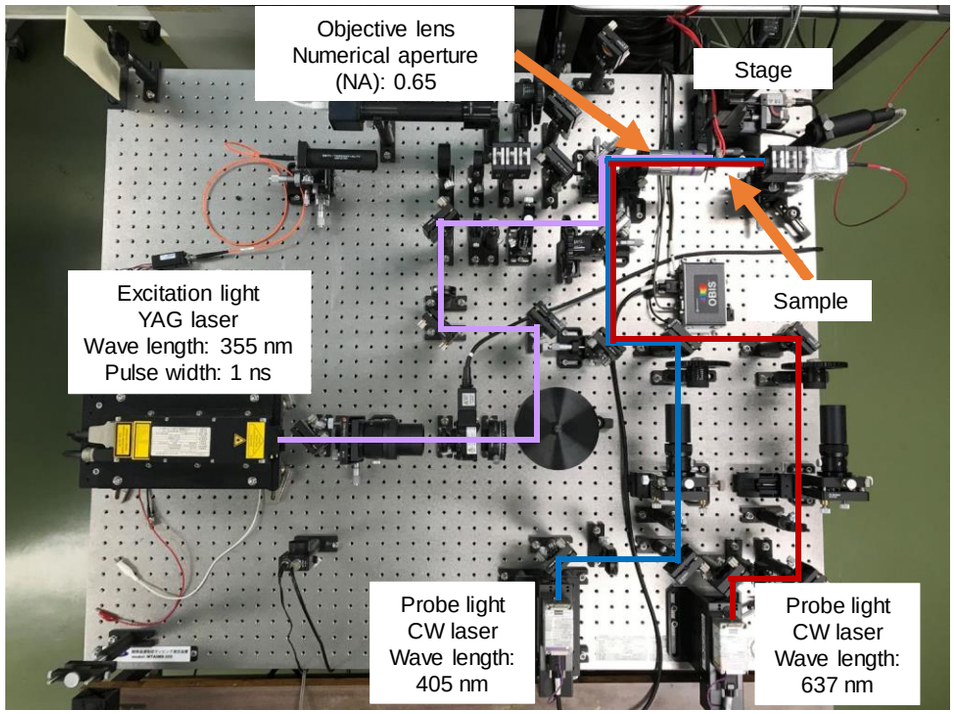

Fig. 3. Photograph of our TRFCA system. By selecting optical paths, we can conduct either intersection or cross-section measurements.

One of the samples applied in this study was the same as that employed in a previous study (wREL)[16], which has a top n^- drift layer (doping concentration of ~1×10^{16} cm^{-3}, thickness of 9.4 μm) and a n^+ buffer layer (REL, doping concentration of ~1×10^{18} cm^{-3}, thickness of 11.1 μm) grown on the Si-face of a 4H-SiC substrate. For a thick epitaxial layer, we employed two samples with an n^- epilayer (nitrogen concentration of ~10^{14} cm^{-3}, thickness of 150 or 250 μm) on the C-face of a 4H-SiC substrate. These were grown under the same conditions as used in a previous study,[23] and we labeled them T-150 and T-250. The carrier lifetime enhancement of these substrates was applied using ion C implantation followed by high-temperature annealing.[24] The cross-section of the samples with the $(1\ \bar{1}00)$ face was treated through mechanical polishing to make a mirror surface for the cross-section measurement. The sample was

mounted a stage with stepper motors with three dimensional movements and the intersection and the cross-section measurements were performed.

Results and discussion

Figure 4 shows a comparison of the 1/e lifetimes obtained from wREL based on the intersection measurements using the previous and present systems. The values of the 1/e lifetimes obtained from the present system are smaller compared with those from the previous system, whereas a decrease in the 1/e lifetime in the n^+ layer (recombination enhancing layer) is more significant for the present system. We consider this difference to be due to larger incident angles of light in the present system. The larger incident angles induce a smaller measurement region. The small measurement region corresponds to a high depth resolution, whereas the excited carriers are easily diffused from the small measurement region, resulting in small 1/e lifetimes. Therefore, the present system has a high depth resolution compared with the previous system.

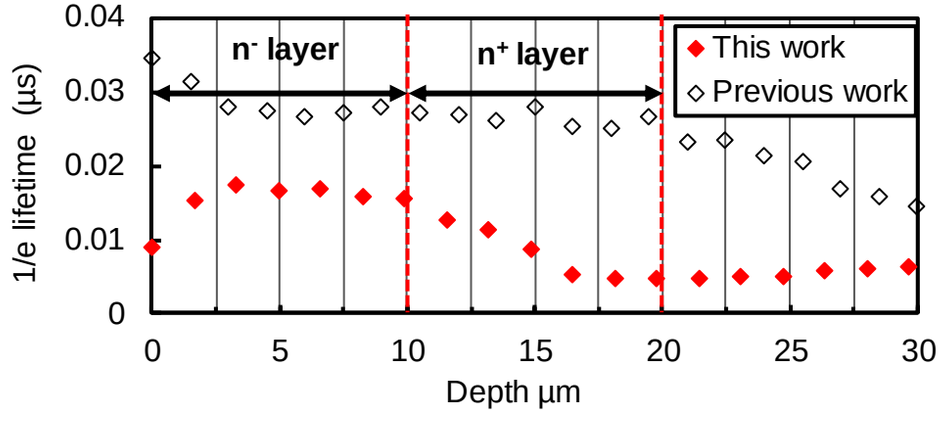

Fig. 4. 1/e lifetime distribution of wREL obtained through the intersection measurements using the previous[16] and present systems.

Figure 5 shows depth-resolved TRFCA decay curves for T-150 and T-250 obtained using the intersection measurements. In this figure, the perspective axis indicates the depth of the samples, which corresponds to the movement distances multiplied by 3.3. The decay curves for T-150 are steep at ~0 and >150 μm, whereas the decay curves for T-250 are steep at ~0, 130, and >250 μm. Figure 5 shows the depth-resolved TRFCA decay curves for T-150 and T-250 obtained using cross-section measurements. Similar to the intersection measurements, the decay curves for T-150 are steep at ~0 and >150 μm, whereas the decay curves for T-250 are steep at ~0 and >250 μm.

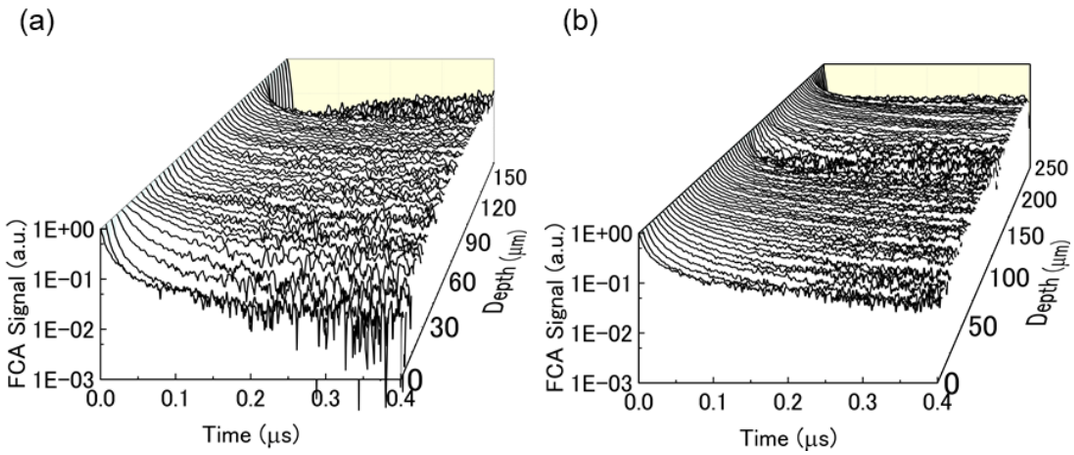

Fig. 5. Depth-resolved FCA decay curves for (a) T-150 and (b) T-250 in the intersection measurements.

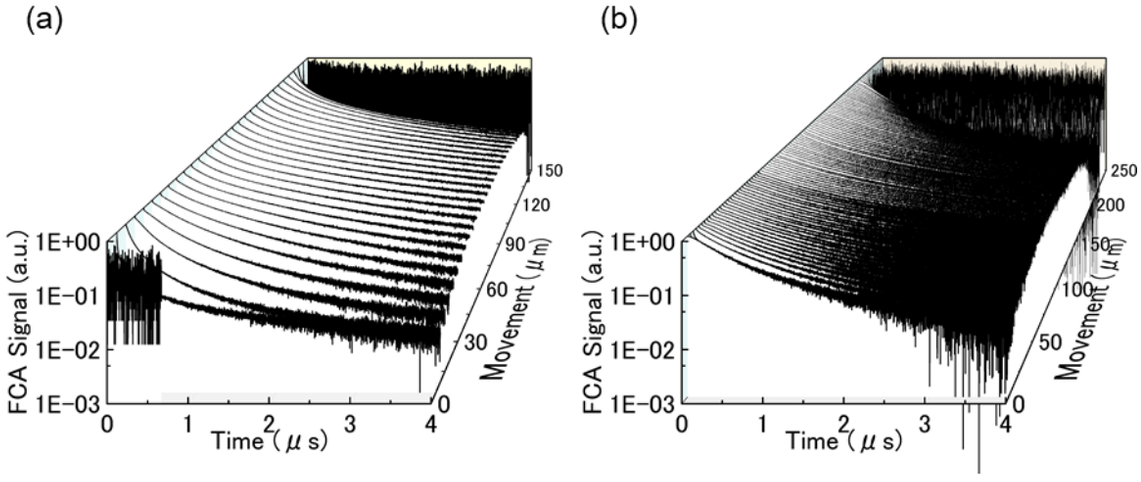

Fig. 6. Depth-resolved FCA decay curves for (a) T-150 and (b) T-250 in the cross-section measurements.

Figure 7 shows the depth distributions of the 1/e lifetimes for T-150 and T-250 obtained from the decay curves shown in Figs. 5 and 6. The 1/e lifetimes from the intersection measurements were significantly smaller than those in the cross-section measurements for both samples, which is due to the diffusion of the excited carriers from the measurement region for the intersection measurements. However, for both measurements, relatively small 1/e lifetimes were observed near the surface (0 μm) and substrate (150 or 250 μm) compared with those in the middle of the epilayers. The small 1/e lifetimes near the surface are due to the surface recombination,[25] whereas the lifetime near the substrate is due to a fast recombination in the substrate. For T-150, the distribution of the 1/e lifetimes based on the cross-section measurements was uniform within the epilayer, while those based on the intersection measurements show a slightly nonuniform distribution of 20–100 μm. We consider this nonuniformity to be caused by a poorer signal-to-noise ratio in the intersection measurements compared with the cross-section measurements. By contrast, for T-250, the 1/e lifetimes at ~130 μm are slightly small in both measurements. The epitaxial growth for T-250 was conducted through two separate runs owing to the requirement of a long growth period for such a thick layer (~125 + ~125 μm). Therefore, the crystal growth condition at ~125 μm will

show slight unintentional differences from the other regions of the epitaxial layer, and densities of point defects, dislocations or stacking faults may be high at ~125 μm. Considering the differences between the intersection and cross-section measurements for these samples, although the 1/e lifetimes by the intersection measurements are smaller and have a slightly poor signal-to-noise ratio compared with those determined through the cross-section measurements, the relative distribution of the 1/e lifetimes was almost the same for both measurements. Therefore, the intersection measurements were able to obtain the carrier lifetime distribution in such thick epilayers. We consider that even if the diffusion of the excited carriers is the dominant mechanism in the IL-TRFCA signal decay, the rate of the diffusion will be fast around the local short carrier lifetime region which will act as a sink of the excited carriers. Therefore, we were able to observe the carrier lifetime distribution as distribution of the 1/e lifetime of the IL-TRFCA signals. The similar lifetime distributions from IL-TRFCA and the cross-section measurements implies that the measurement results of IL-TRFCA were reliable, and this confirmation of the measurement reliability is the first time for the nondestructive carrier lifetime measurements.[15,16]

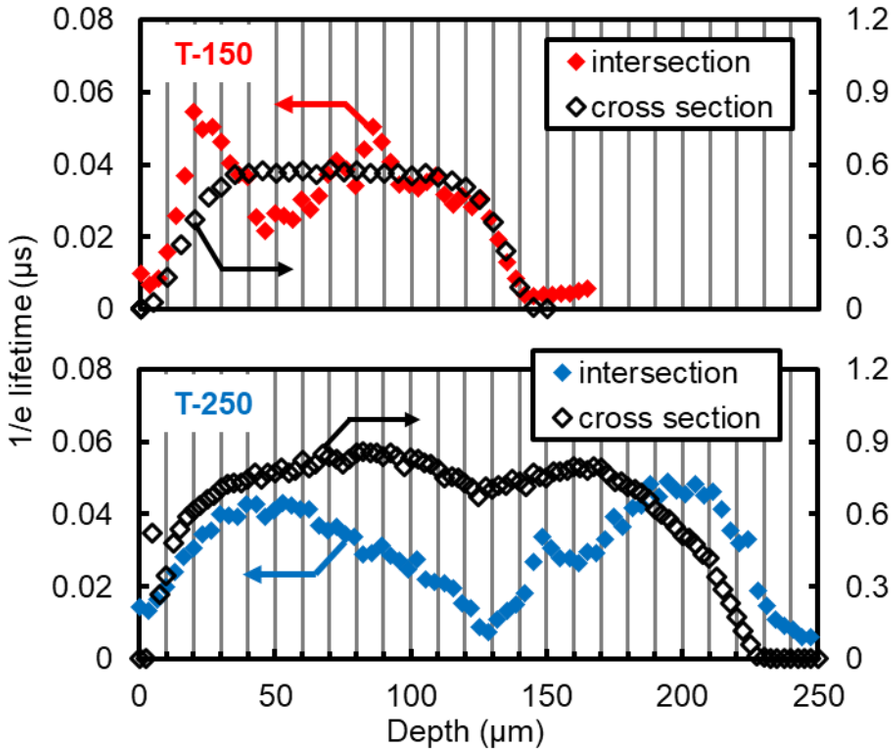

Fig. 7. Depth distributions of 1/e lifetime for T-150 and T-250. The upper plot is for T-150 and the lower plot is for T-250. The red and blue colored symbols are for the intersection measurements, and the black symbols are for the cross-section measurements.

A quantitative discussion of the depth spatial resolution of the intersection measurements is important to clarify the usefulness of IL-TRFCA. As seen at the surfaces or epilayer/substrate interfaces shown in Fig. 7, the intersection and cross-section measurements demonstrate almost the same 1/e lifetime distributions. Therefore, the intersection measurements may have almost the same spatial resolution as the cross-section measurements (~10 μm), although the resolution depends on the diffusion length of the excited carriers. On the other hand, the dip of the 1/e lifetime at the middle of the epilayer in T-250 show much broader than 10 μm. Origins of this broadness are not clear, but the second epitaxial growth on the first epilayer might induce dislocation loops such as stacking faults around the epilayer/epilayer interface

which reduced the carrier lifetime around the interface making broad carrier lifetime distribution.[26] By contrast, as shown in Fig. 4, the intersection measurements clearly show relatively long 1/e lifetimes near the surface, and then it gradually reduces from the depth of 10 μm and reaches the minimum value at 17 μm. It has been confirmed that the n^- layer has longer carrier lifetime than the recombination enhancing layer from the depth of 9.4 μm.[10] Therefore, IL-TRFCA resolved the carrier lifetime distribution of the n^- layer with ~10 μm which corresponds to the depth resolution estimated from the lifetime distribution around the epilayer/substrate interface in Fig. 7. When compared with the TPA-TRPL measurements, the TPA-TRPL measurements excite the carriers within a range of 10 μm in the depth direction, and to obtain an accurate carrier lifetime, the fittings of the decay curves were conducted under a decay period of almost twice the carrier lifetime.[15] Therefore, the TPA-TRPL signal includes information from a region with twice the diffusion length, which is typically larger than 10 μm, and thus IL-TRFCA has an advantage in terms of the spatial resolution, as described above. Both nondestructive depth-resolved techniques will complement the development of SiC devices with a carrier lifetime distribution in the epitaxial layers.

Conclusions

We have developed and improved an IL-TRFCA system for the nondestructive measurements of the depth distribution of the carrier lifetime in 4H-SiC thick epilayers. Compared with our previous system, we employed higher NA objective and detection lenses and increased the incident angles of the lights. To confirm reliability of the measurement results, we also performed TRFCA measurements to cross-section of the samples. As a result, although the values of the lifetimes obtained by IL-TRFCA were underestimated owing to an inevitable diffusion of the carriers from the measurement region, the system enables observations of the carrier lifetime distribution up to a depth of 250 μm. Our IL-TRFCA system shows a depth resolution of ~10 μm, which is the best resolution among previously reported

nondestructive measurement techniques. We believe this system will be useful for the development of SiC bipolar devices.

Supplementary Material

See supplementary material for measurement results for the diameters of the lasers at the focal point for IL-TRFCA.

Acknowledgements

This work is supported by SIP (Strategic Innovation Promotion Program) of the Council for Science, Technology and Innovation [(Next generation power electronics / Integrated research and development of SiC for next generation power electronics] (management corporation: NEDO).

Data Availability Statement

The data that support the findings of this study are available from the corresponding author upon reasonable request.

REFERENCES

1. T. Kimoto, Jpn. J. Appl. Phys. **58**, 018002 (2019).
2. M. Saggio, V. Raineri, R. Letor, and F. Frisina, IEEE Electron Device Lett. **18**, 333 (1997).

3. E. van Brunt, L. Cheng, M. J. O'Loughlin, J. Richmond, V. Pala, J. Palmour, C. W. Tipton, and C. Scozzie, Mater. Sci. Forum 821–823, 847 (2015).
4. K. Nakayama, A. Tanaka, M. Nishimura, K. Asano, T. Miyazawa, M. Ito, and H. Tsuchida, IEEE Trans. Electron Devices **59**, 895 (2012).
5. N. Kaji, H. Niwa, J. Suda, and T. Kimoto, IEEE Trans. Electron Devices **62**, 374 (2015).
6. H. Miyake, T. Okuda, H. Niwa, T. Kimoto, and J. Suda, IEEE Electron Device Lett. **33**, 1598 (2012).
7. T. Kimoto and Y. Yonezawa, Mater. Sci. Semicond. Process. **78**, 43 (2018).
8. H. Tsuchida, I. Kamata, T. Miyazawa, M. Ito, X. Zhang, and M. Nagano, Mater. Sci. Semicond. Process. **78**, 2 (2018).
9. M. Saggio, V. Raineri, R. Letor, and F. Frisina, IEEE Electron Device Lett. **18**, 333 (1997).
10. T. Tawara, T. Miyazawa, M. Ryo, M. Miyazato, T. Fujimoto, K. Takenaka, S. Matsunaga, M. Miyajima, A. Otsuki, Y. Yonezawa, T. Kato, H. Okumura, T. Kimoto, and H. Tsuchida, J. Appl. Phys. **120**, 115101 (2016).
11. P. Grivickas, A. Galeckas, J. Linnros, M. Syväjärvi, R. Yakimova, V. Grivickas, and J.A. Tellefsen, Mater. Sci. Semicond. Process. **4**, 191 (2001).
12. V. Grivickas, G. Manolis, K. Gulbinas, K. Jarašiūnas, and M. Kato, Appl. Phys. Lett. **95**, 242110 (2009).
13. A. Galeckas, O. Tomblad, J. Linnros, and B. Breitholtz, IEEE Electron Device Lett. **20**, 295 (1999).
14. A. Galeckas, J. Linnros, M. Frischholz, and V. Grivickas, Appl. Phys. Lett. **79**, 365 (2001).
15. N.A. Mahadik, R.E. Stahlbush, P.B. Klein, A. Khachatrian, S. Buchner, G. Steven, N.A. Mahadik, R.E. Stahlbush, P.B. Klein, and A. Khachatrian, Appl.Phys. Lett. **111**, 221904 (2017).
16. S. Mae, T. Tawara, H. Tsuchida, and M. Kato, Mater. Sci. Forum **924**, 269 (2018).

17. S. Zollner, J.G. Chen, E. Duda, T. Wetteroth, S.R. Wilson, and J.N. Hilfiker, J. Appl. Phys. **85**, 8353 (1999).
18. N. Watanabe, T. Kimoto, and J. Suda, Jpn. J. Appl. Phys. **53**, 108003 (2014).
19. K. Neimontas, T. Malinauskas, R. Aleksiejūnas, M. Sūdžius, K. Jarašiūnas, L. Storasta, J.P. Bergman, and E. Janzen, Semicond. Sci. Technol. **21**, 952 (2006).
20. S. Limpijumnong, W. Lambrecht, S. Rashkeev, and B. Segall, Phys. Rev. B **59**, 12890 (1999).
21. P. Grivickas, K. Redeckas, K. Gulbinas, A. M. Conway, L. F. Voss,1 M. Bora, S. Sampayan, M. Vengris, and V. Grivickas, J. Appl. Phys. **125**, 225701 (2019).
22. K. Nagaya, T. Hirayama, T. Tawara, K. Murata, H. Tsuchida, A. Miyasaka, K. Kojima, T. Kato, H. Okumura, M. Kato, J. Appl. Phys. 128, 105702 (2020).
23. M. Kushibe, J. Nishio, R. Iijima, A. Miyasaka, H. Asamizu, H. Kitai, R. Kosugi, S. Harada, and K. Kojima, Mater. Sci. Forum **432-435**, 924 (2018).
24. L. Storasta, and H. Tsuchida, Appl. Phys. Lett. **90**, 062116 (2007).
25. M. Kato, Z. Xinchi, K. Kohama, S. Fukaya, and M. Ichimura, J. Appl. Phys. **127**, 195702 (2020).
26. M. Kato, S. Katahira, Y. Ichikawa, S. Harada, and T. Kimoto, J. Appl. Phys. **124**, 095702 (2018).

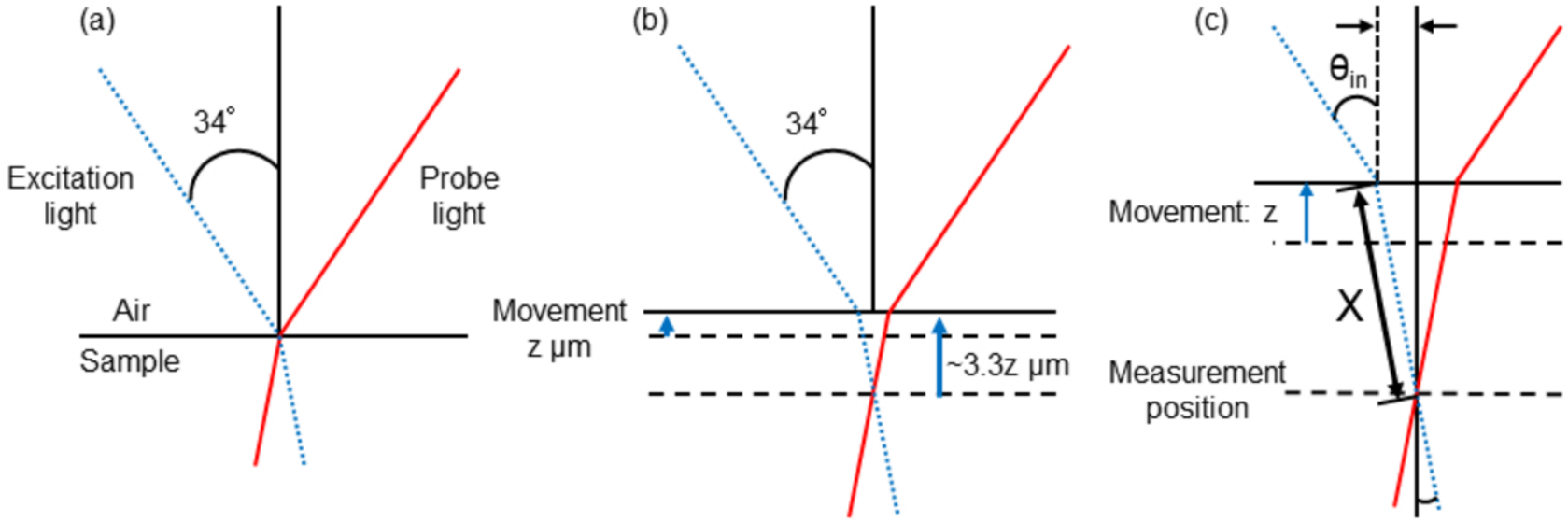
(a)
34˚
Excitation light
Probe light
Air
Sample
(b)
34˚
Movement z μm
~3.3z μm
(c)
θin
Movement: z
X
Measurement position

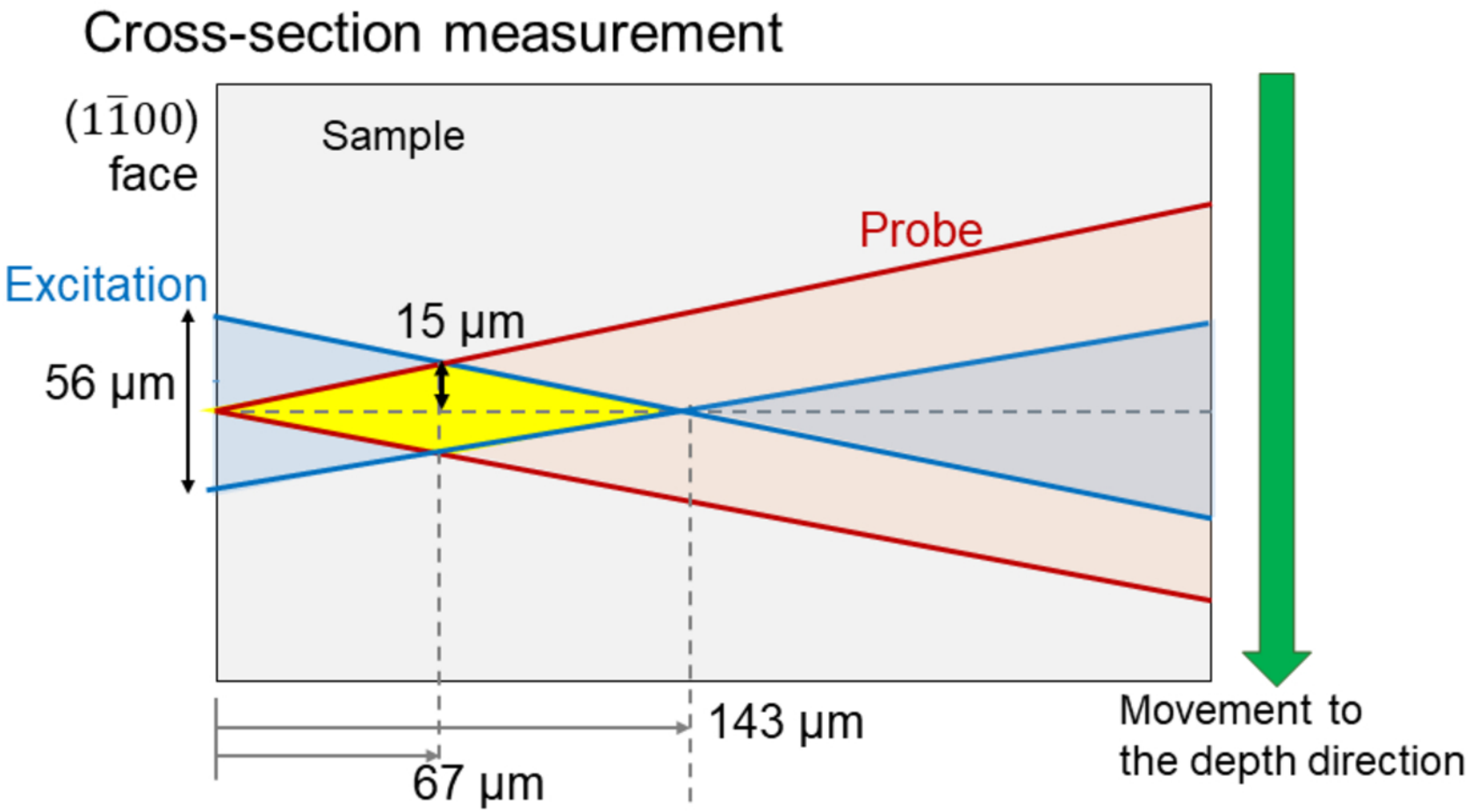
Cross-section measurement
$(1\bar{1}00)$ face
Sample
Probe
Excitation
15 μm
56 μm
143 μm
67 μm
Movement to the depth direction

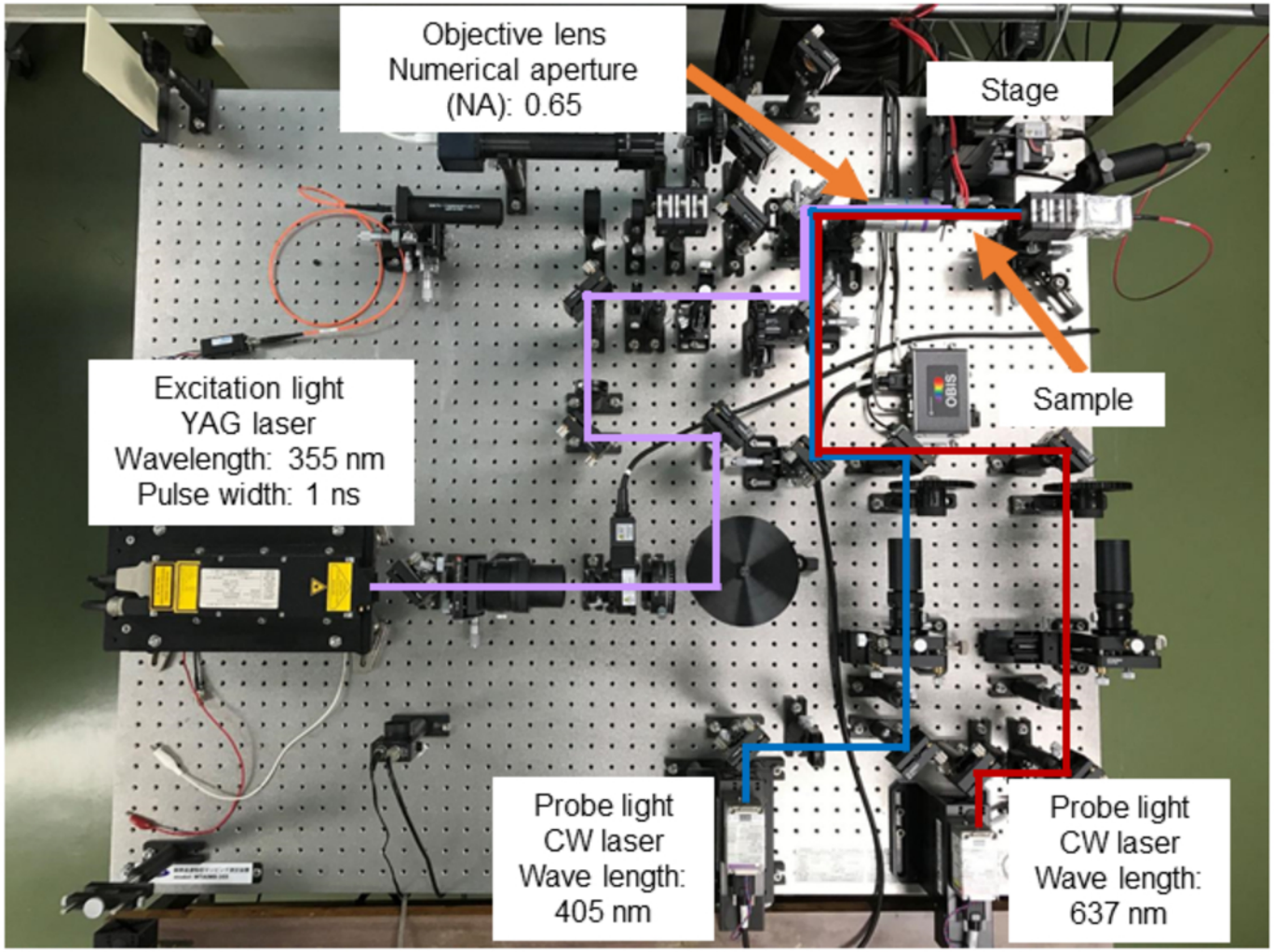
Objective lens
Numerical aperture
(NA): 0.65
Stage
Excitation light
YAG laser
Wavelength: 355 nm
Pulse width: 1 ns
Sample
Probe light
CW laser
Wave length:
405 nm
Probe light
CW laser
Wave length:
637 nm

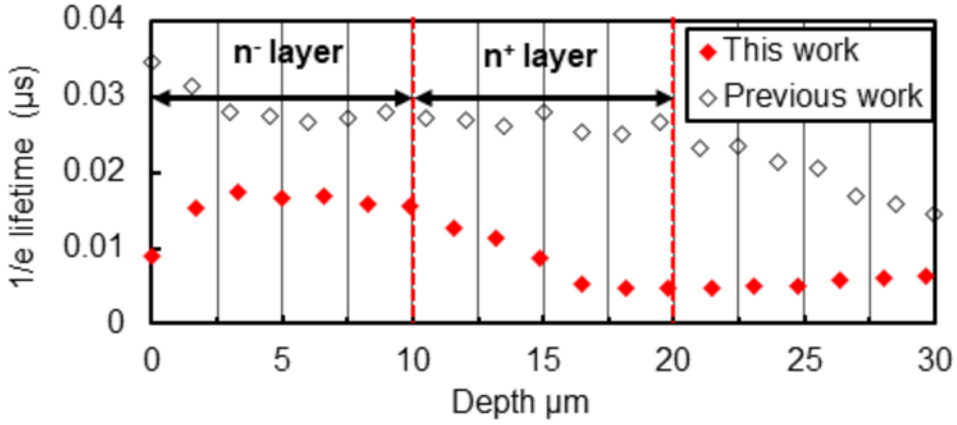
0.04
0.03
0.02
0.01
0
1/e lifetime (μs)
n⁻ layer
n⁺ layer
This work
Previous work
0
5
10
15
20
25
30
Depth μm

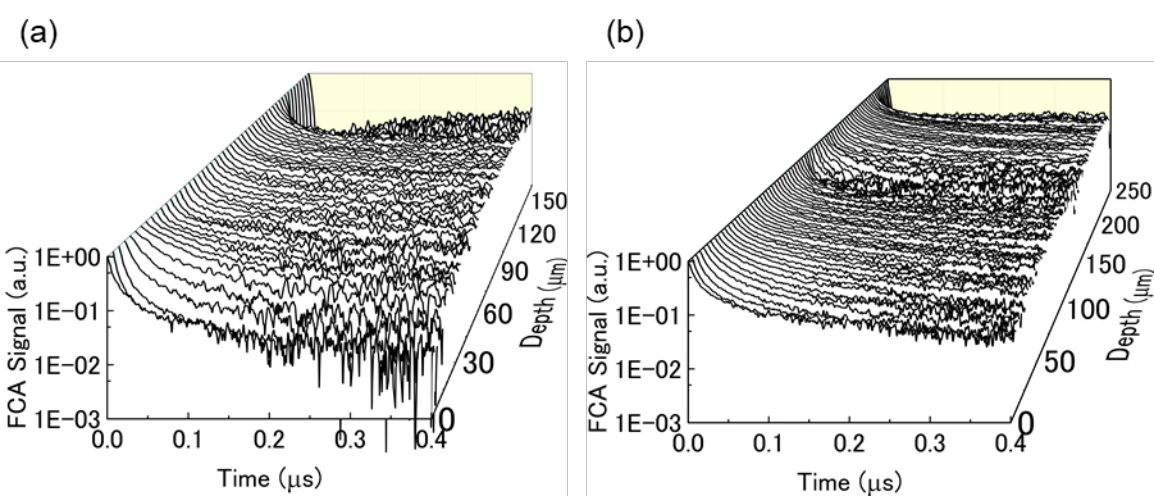
(a)
(b)
FCA Signal (a.u.)
1E+00
1E-01
1E-02
1E-03
0.0
0.1
0.2
0.3
0.4
Time (μs)
Depth (μm)
150
120
90
60
30
0
250
200
150
100
50
0

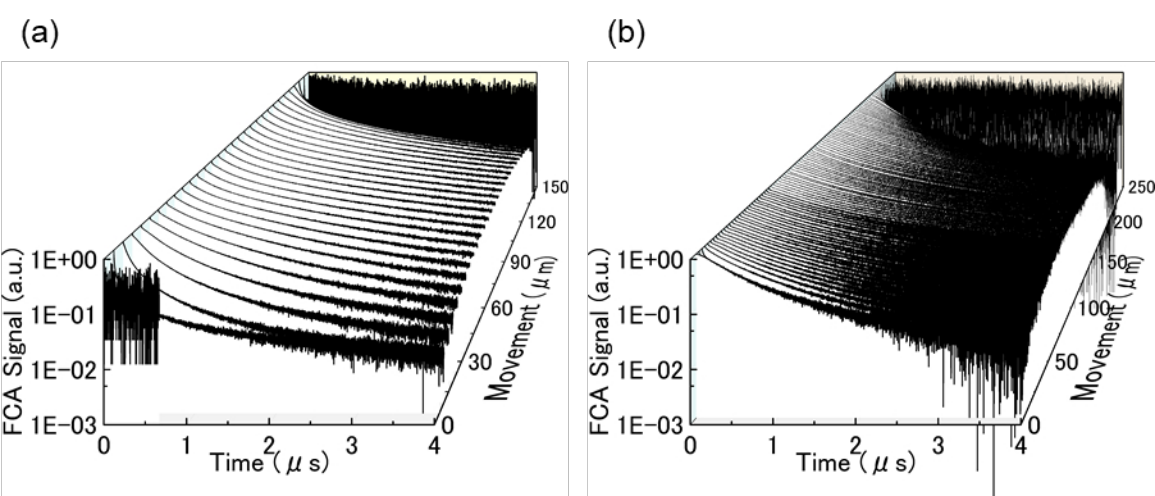
(a)
(b)
FCA Signal (a.u.)
1E+00
1E-01
1E-02
1E-03
0
1
2
3
4
Time (μ s)
Movement (μ m)
150
120
90
60
30
0
250
200
150
100
50
0

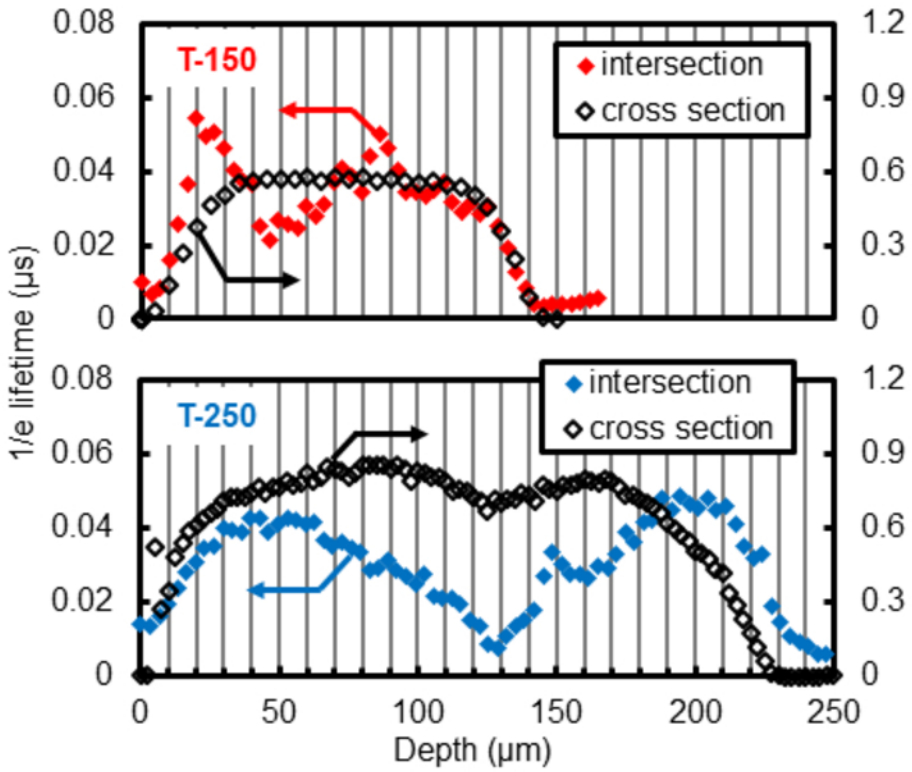
T-150
intersection
cross section
T-250
intersection
cross section
1/e lifetime (μs)
Depth (μm)
0.08
0.06
0.04
0.02
0
1.2
0.9
0.6
0.3
0
0
50
100
150
200
250